

60 GHz Tapered Transmission Line Resonators

*Cristian Marcu
Ali Niknejad*



Electrical Engineering and Computer Sciences
University of California at Berkeley

Technical Report No. UCB/EECS-2008-117

<http://www.eecs.berkeley.edu/Pubs/TechRpts/2008/EECS-2008-117.html>

September 15, 2008

Copyright 2008, by the author(s).
All rights reserved.

Permission to make digital or hard copies of all or part of this work for personal or classroom use is granted without fee provided that copies are not made or distributed for profit or commercial advantage and that copies bear this notice and the full citation on the first page. To copy otherwise, to republish, to post on servers or to redistribute to lists, requires prior specific permission.

Acknowledgement

The authors would like to thank the BWRC sponsors, NSF Infrastructure Grant No. 0403427, wafer fabrication donation by STMicroelectronics, DARPA TEAM program (contract no. DAAB07-02-1-L428), Motorola, and the UC-Micro program.

60 GHz Tapered Transmission Line Resonators

by Cristian Marcu

Research Project

Submitted to the Department of Electrical Engineering and Computer Sciences,
University of California at Berkeley, in partial satisfaction of the requirements for the
degree of **Master of Science, Plan II**.

Approval for the Report and Comprehensive Examination:

Committee:

Professor Ali M. Niknejad
Research Advisor

(Date)

* * * * *

Professor Elad Alon
Second Reader

(Date)

Contents

List of Figures	ii
List of Tables	iv
1 Introduction	1
2 Tapered Transmission Line Resonators	7
2.1 Tapering Principle	7
2.2 Transmission Line Equations	9
2.3 Taper Optimization	11
2.3.1 EM Model Extraction	12
2.3.2 Optimization Methodology	17
2.3.3 Optimization Results	20
2.4 Experimental Results	22
2.4.1 Accounting for Deembedding Inaccuracies	27
2.5 Comparison to lumped LC tank	30
3 Conclusion	33
Bibliography	36

List of Figures

1.1	Cross-coupled differential pair VCOs with LC tank (left) and quarter wavelength transmission line resonators (right).	3
2.1	The current and voltage standing wave ratio on a lossless quarter wave transmission line.	8
2.2	A tapered quarter wave transmission line utilizes wide width and large gap spacing when the current is high (voltage is low) and narrow width and small gap when the voltage is high (current is low).	8
2.3	RLGC ladder representation of a transmission line.	9
2.4	Uniform shorted differential stripline.	12
2.5	Characteristic impedance of differential stripline.	13
2.6	$RLGC$ per meter for a uniform differential stripline.	15
2.7	Resonant Q of quarter wavelength uniform differential stripline.	17
2.8	Tapered resonator optimization flow chart.	19
2.9	The layout of the optimized quarter wave line. The characteristic impedance Z_0 is non-constant. Slotting is introduced to satisfy design rules.	20
2.10	The optimum characteristic impedance Z_0 profile.	20
2.11	The layout of the optimized capacitor loaded half-resonator. The characteristic impedance Z_0 is non-constant. Slotting is introduced to satisfy design rules.	21
2.12	Layout of resonator test structures.	23
2.13	Layout of deembedding structure.	24
2.14	Measured and simulated impedance for the uniform resonator.	25
2.15	Measured and simulated impedance for the tapered resonator.	26
2.16	Measured and simulated impedance for the capacitor-loaded tapered half-resonator. (Capacitor Q is assumed to be 40 in simulation.)	26
2.17	Tapered resonator 3D layout model in HFSS including undeembedded interconnect and microstrip to CPS transition. The two insets show the actual extent of deembedding (left) compared to the expected deembedding (right).	28
2.18	Measured and simulated impedance for the tapered resonator taking into account the deembedding structure layout error.	29
2.19	Single turn octagonal inductor layout in HFSS using only the top metal layer.	31

2.20	Simple inductor model taking into account series losses.	31
2.21	Inductive Q versus inductance comparison between standard single turn octagonal inductors and tapered half-resonator.	32
3.1	A tapered open ended half wave transmission line utilizes wide width and large gap spacing when the current is high (voltage is low) and narrow width and small gap when the voltage is high (current is low).	34

List of Tables

2.1	Measurement Results	26
-----	-------------------------------	----

Acknowledgments

The authors would like to thank the BWRC sponsors, NSF Infrastructure Grant No. 0403427, wafer fabrication donation by STMicroelectronics, DARPA TEAM program (contract no. DAAB07-02-1-L428), Motorola, and the UC-Micro program.

Chapter 1

Introduction

Millimeter-wave transceivers require a local reference frequency for upconversion from baseband to RF for transmission, or downconversion of received RF signals down to baseband. This reference can also be divided down to a lower frequency for use as the baseband clock signal. Voltage controlled oscillators (VCOs) can provide this local frequency reference either as free-running oscillators or locked to a stable reference using phase locked loops. Typically, VCOs which utilize a resonant tank achieve the best overall performance, and thus are very common in mm-wave applications. The design of CMOS mm-wave VCOs, however, involves a complex set of trade-offs between tuning range, phase noise, DC power consumption, and output power. In many cases, the most important of these metrics are tuning range and phase noise. The tuning range of the VCO must be large enough to cover the desired band of interest taking into account process, voltage, and temperature variations as well as modelling inaccuracies. Phase noise, on the other hand, contributes to the overall noise figure of the transceiver by causing downconversion of

noise and any undesired signals located in frequencies adjacent to the desired signal. Both metrics, however, are strongly dependent on the type and quality factor of the resonant tank used, as shown by Leeson's well known equation for the phase noise of an oscillator [1].

$$L\{\Delta\omega\} = 10\log \left[S(\Delta\omega) \left\{ 1 + \frac{\omega_0}{2Q\Delta\omega} \right\} \right] \quad (1.1)$$

Even though this equation is based on an LTI approximation, it gives valuable insight into the design parameters. For example, we can see that in order to minimize oscillator phase noise, a high Q resonant tank must be used.

The most common tank is simply a parallel LC tank. Usually the tank inductance is kept constant since it is very difficult to tune an inductor, and the tuning comes from changing the capacitance value. This can be accomplished either by switching in and out small capacitors, using varactors for part of the capacitance, or both. However, at high frequencies the size of these lumped components begins to approach an appreciable fraction of the wavelength, and thus these lumped components begin to exhibit distributed behavior.

Transmission lines are a necessary component of high frequency and mm-wave designs because they explicitly take into account this distributed behavior. They can be used not only to carry signals, but also as reactive components and resonators. This work focuses on their use as resonators for 60 GHz CMOS applications and seeks to achieve higher resonant quality factors than what is achievable with lumped components.

A quarter-wavelength of transmission line shorted at one end looks like an open circuit from the opposite end and thus behaves like a parallel LC tank. By applying a negative resistance, such as a cross-coupled differential pair, this transmission line can be used to create an oscillator as shown in Fig. 1.1. A signal travels from the negative resistance

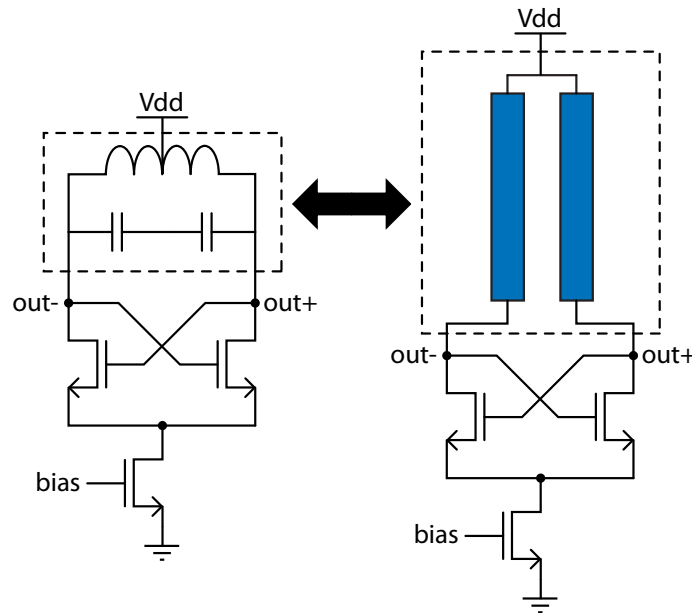


Figure 1.1: Cross-coupled differential pair VCOs with LC tank (left) and quarter wavelength transmission line resonators (right).

cell to the shorted end of the line where it is reflected and travels back to the source. The sum of these two travelling waves forms a standing wave pattern along the transmission line. It is this standing wave behavior of such an oscillator which can be exploited to lower losses along the line through the use of tapering.

The idea of tapering a transmission line has been studied and used extensively in the microwave community for many years as a way to provide a conjugate match between two sections of transmission line with different characteristic impedances. Initially this work began as a cascade of quarter-wavelength sections of transmission line with different characteristic impedances, also known as quarter-wavelength transformers due to their impedance transformation characteristics, and evolved into single tapered sections of line. As early as the 1930s many authors had worked out solutions for the behavior of a tapered

transmission line with characteristic impedance profiles that varied in a specified manner (ie: exponential, Gaussian, etc.). However, Collin, [2] was the first to produce an analysis of what constitutes an optimum taper and the synthesis of such a taper. The results of this work showed that the optimal synthesis described obtained better performance than comparable exponential or Gaussian tapers.

Recently, the idea of tapering has resurged in microwave integrated circuits. Due to the presence of lossy substrates and the expense associated with RF process options such as thick top metal layers far away from the substrate, CMOS designers have a very hard time designing high quality factor inductors for mm-wave VCOs. However, at such high frequencies it becomes possible to use on-chip transmission lines which utilize a reasonable amount of area. The most popular forms of integrated transmission lines have been microstrip, coplanar waveguide (CPW), and coplanar stripline (CPS). Microstrip lines offer great flexibility in layout and effectively shield the signals from the lossy substrate. However, the ground plane must be placed in a thin, low metal layer, thus increasing the loss. This is due to the fact that the characteristic impedance is mainly determined by the ratio of signal width to the distance between signal and ground. Thus, the ground and signal must be placed as far apart as possible to allow the use of wide signal lines. Coplanar waveguides have both the signal and ground lines in the topmost thick metal layer and thus tend to provide lower loss for small spacings. The characteristic impedance is determined by both the signal width and the spacing between the signal and ground lines, however, it is most sensitive to the spacing. Unfortunately, as the spacing is increased, more fields penetrate the substrate and thus the loss increases. The coplanar stripline is similar to a coplanar

waveguide in that both signals are in the topmost thick metal layer and suffer from the same spacing limitation. However, the coplanar stripline is inherently a differential structure and thus lends itself very well to the design of quarter wavelength resonators for VCOs. Moreover, the differential characteristic impedance has a similar dependence on both the width of the signal lines and their spacing.

Andress first proposed the idea of tapering a differential CPS transmission line resonator to reduce its loss and thus enhance its quality factor [3]. The characteristic impedance was kept constant to eliminate internal reflections and simplify the synthesis of an optimal taper. Similarly, Krishnaswamy utilized a CPS transmission line with shielding to create a very high quality factor inductor [4]. Due to the large spacing required to get the necessary inductance, the author devised an optimal taper to interface to the much smaller active cell of the VCO core.

This work builds on [3] by removing the constraint on characteristic impedance. If the characteristic impedance of the line is kept constant along its length, the voltage and current waveforms in the phase domain are sinusoidal in shape regardless of the shape of the line, allowing a relatively straightforward optimization. However, this approach is theoretically limited to a 60% improvement in quality factor Q over the uniform resonator. By removing the constraint on the characteristic impedance, this work achieves further improvements in Q , limited only by the substrate losses. Determining the optimum taper shape is however a complex multi-dimensional optimization problem made more difficult by the fact that the characteristic impedance profile can vary arbitrarily. Thus, the voltage and current waveforms cannot be derived analytically and a numerical approach must be

used in the optimization.

The optimization results in a resonator with very narrow width for much of its length. In a usual VCO implementation like the one shown in Fig. 1.1, the resonator would be used to bias up the VCO core and would thus need to carry DC current. With this in mind, the narrow section can be removed and replaced with a capacitor. In this way, the shorted length of transmission line is being used as an inductor as in [4]. This tapered, capacitor-loaded half-resonator can exhibit higher quality factor than the full resonator depending on the quality of the lumped capacitor used and still maintains the optimal behavior of the full taper. As a final note, this work explores the benefits that this optimization can provide as a function of frequency, leading to a conclusion on its possible applications.

Chapter 2

Tapered Transmission Line Resonators

2.1 Tapering Principle

A differential stripline shorted at one end exhibits the standing wave mode shown in Fig. 2.1 at resonance. At the shorted end of the line, the voltage is at a minimum and the current at a maximum, so the losses at this point come mainly from the series resistance of the metal line. Conversely, at the driven end, the voltage is at a maximum and the current at a minimum, so the losses at this point come mainly from the shunt conductance between the differential lines. This phenomenon can be exploited to lower the losses of the resonator and thus raise the quality factor [3]. At the shorted end of the line, the metal conductors can be made wider to reduce the series resistance without having to worry about the increase in shunt conductance. The gap spacing can also be made wide since the voltage difference

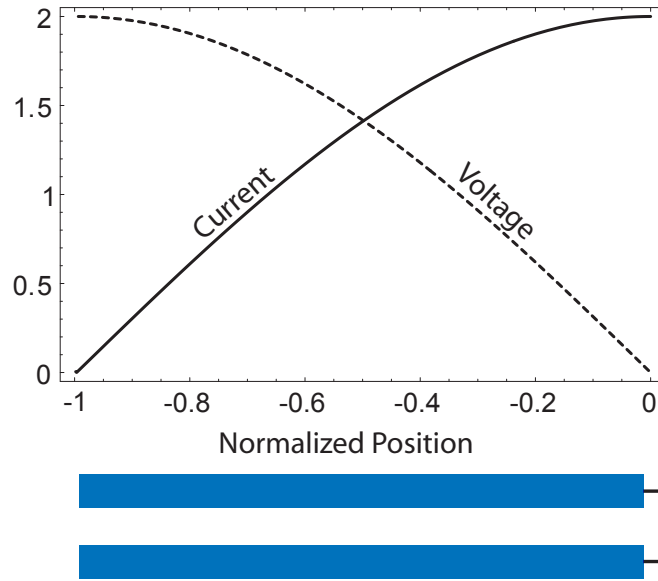


Figure 2.1: The current and voltage standing wave ratio on a lossless quarter wave transmission line.

between the lines is small. Similarly, at the driven end of the line, the conductors can be made very narrow to lower the conductance without having to worry about the increase in series resistance. The gap spacing should be small in order to minimize field leakage into the substrate since the fields are strongest at this end of the line. Along the rest of the line, shunt conductance and series resistance can be traded off to achieve a tapered line with



Figure 2.2: A tapered quarter wave transmission line utilizes wide width and large gap spacing when the current is high (voltage is low) and narrow width and small gap when the voltage is high (current is low).

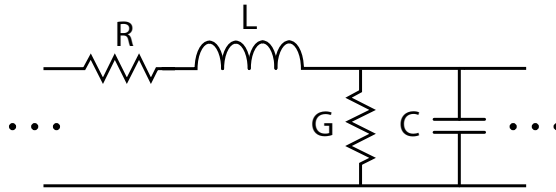


Figure 2.3: RLGC ladder representation of a transmission line.

much lower losses than the optimum uniform line. The optimum taper shape should thus end up looking similar to Fig. 2.2.

2.2 Transmission Line Equations

Any transmission line can be represented by a distributed *RLGC* ladder network as shown in Fig. 2.3, the electrical characteristics of which are described by the well known Telegrapher's Equations [5], [6].

$$\frac{dV(x)}{dx} = -(R(x) + j\omega L(x)) \cdot I(x) \quad (2.1)$$

$$\frac{dI(x)}{dx} = -(G(x) + j\omega C(x)) \cdot V(x) \quad (2.2)$$

Combining the above two equations and assuming low loss conditions ($R = G = 0$) leads to a differential equation representation of an arbitrary transmission line in the voltage domain [7], [8]

$$\frac{d^2V(x)}{dx^2} - \frac{1}{L(x)} \frac{dL(x)}{dx} \frac{dV(x)}{dx} - \omega^2 L(x) C(x) V(x) = 0 \quad (2.3)$$

$$I(x) = -\frac{1}{j\omega L(x)} \cdot \frac{dV(x)}{dx} \quad (2.4)$$

or in the current domain

$$\frac{d^2 I(x)}{dx^2} - \frac{1}{C(x)} \frac{dC(x)}{dx} \frac{dI(x)}{dx} - \omega^2 L(x) \cdot C(x) \cdot I(x) = 0 \quad (2.5)$$

$$V(x) = -\frac{1}{j\omega C(x)} \cdot \frac{dI(x)}{dx} \quad (2.6)$$

Previous work [3] has shown that the transforms defined in Eq. 2.7 and Eq. 2.8

$$L_\theta(\theta) = \frac{L(x)}{\beta(x)} = \frac{L(x)}{\omega \sqrt{L(x)C(x)}} = \frac{1}{\omega} \sqrt{\frac{L(x)}{C(x)}} = \frac{Z_0(x)}{\omega} \quad (2.7)$$

$$C_\theta(\theta) = \frac{C(x)}{\beta(x)} = \frac{C(x)}{\omega \sqrt{L(x)C(x)}} = \frac{1}{\omega} \sqrt{\frac{C(x)}{L(x)}} = \frac{1}{\omega Z_0(x)} \quad (2.8)$$

can be used to convert the transmission line equations presented above from the physical domain to the phase domain described by

$$\theta(x) = \int_0^x \beta(x') dx' = \int_0^x \omega \sqrt{L(x')C(x')} dx' \quad (2.9)$$

Under these transforms Eq. 2.3 becomes

$$\frac{d^2 V(\theta)}{d\theta^2} - \frac{1}{Z_0(\theta)} \frac{dZ_0(\theta)}{d\theta} \frac{dV(\theta)}{d\theta} - V(\theta) = 0 \quad (2.10)$$

whose solution can be found analytically if the characteristic impedance profile is well behaved (ie.: constant [3], linear [9], exponential [8], etc.). For example, if the characteristic impedance is kept constant, the second term in Eq. 2.10 goes to zero and the dependence of the voltage profile on characteristic impedance, and thus on the shape of the taper, completely drops out leading to Eq. 2.11.

$$\frac{d^2 V(\theta)}{d\theta^2} - V(\theta) = 0 \quad (2.11)$$

The solution to this differential equation is a sinusoid. However, if the characteristic impedance is allowed to vary, as in this work, the voltage profile is a complex function

of the taper shape even in the phase domain. Therefore, from this point on we elect to use Eqs. 2.3 and 2.4, the equations for voltage in the physical domain, since working in the phase domain provides no advantages. Due to the fact that the characteristic impedance profile is not known and can vary arbitrarily, Eqs. 2.3 and 2.4 are nonlinear and cannot be solved analytically [8]. Instead, we turn to a numerical solution. A Matlab script was developed to solve for the voltage and current waveforms along an arbitrary transmission line for which the $L(x)$ and $C(x)$ profiles are known. This script numerically solves Eq. 2.3 and 2.4 with boundary conditions of $V(0) = 1$ and $V'(0) = 0$. The resonant quality factor can then be calculated by computing the ratio of energy stored to energy dissipated per cycle using Eq. 2.12.

$$Q = \omega \frac{E_{\text{stored}}}{P_{\text{diss}}} = \omega \frac{\int_0^\ell \frac{1}{4} (V^2(x)C(x) + I^2(x)L(x)) dx}{\int_0^\ell \frac{1}{2} (V^2(x)G(x) + I^2(x)R(x)) dx} \quad (2.12)$$

2.3 Taper Optimization

The goal of this optimization is maximizing the resonant quality factor. Thus, we can see from Eq. 2.12 that this means maximizing energy storage while minimizing energy losses. The taper optimization is accomplished with the help of Momentum, a 2.5D EM simulator, HFSS, a 3D EM simulator, and Matlab. Momentum and HFSS were first used to extract *RLGC* models for differential strip lines of varying widths and spacings covering the desired design space. The transmission line *RLGC* model was chosen over the Z_0 and Γ model since it provides more intuition for this particular optimization. It is relatively easy to explain changes in resistance, inductance, conductance, and capacitance based on layout changes as opposed to determining changes in Z_0 or Γ . Furthermore, the optimization is

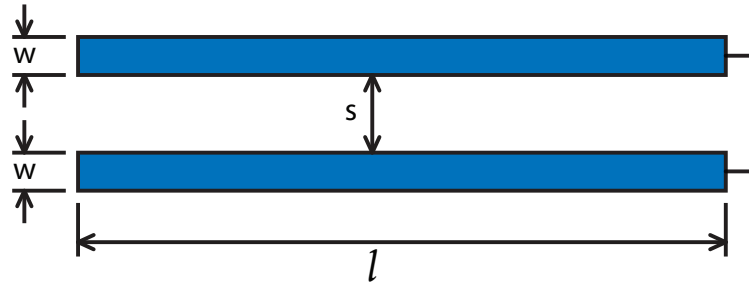


Figure 2.4: Uniform shorted differential stripline.

based exactly on understanding how layout changes affect energy losses, due to resistance and conductance, and energy storage, due to inductance and capacitance. Matlab was used to actually run the optimizations and, finally, HFSS and Momentum were used to simulate the resulting taper shape to verify the optimization results.

2.3.1 EM Model Extraction

Momentum, which is a 2.5D EM simulator, was chosen for EM model extraction due to its speed when simulating simple structures. The technology used for the transmission line implementation is a standard digital 90nm CMOS process in which we used the top metal layer. The planar nature of this process allows us to use Momentum with little or no loss of accuracy when compared to a full 3D simulator such as HFSS. However, the full substrate stack is made up of many oxide layers with different EM characteristics. To speed up simulation time it is imperative to simplify the substrate stackup dramatically. This was achieved by using only one oxide layer which encompasses all metal layers. The characteristics of this oxide layer and the silicon substrate below were matched to measurements of CPW transmission lines with varying widths and spacings.

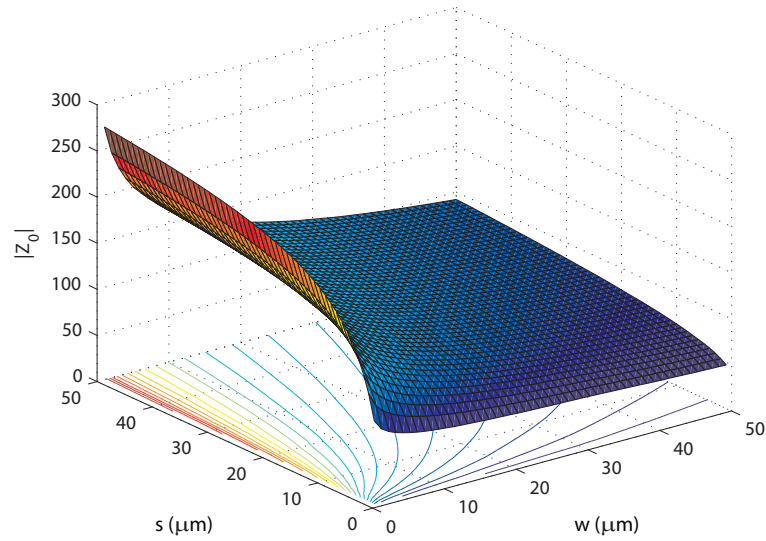


Figure 2.5: Characteristic impedance of differential stripline.

The simulation setup used a length of CPS transmission line, similar to the one shown in Fig. 2.4, with variable conductor width, spacing, and length but without one end shorted. One port was placed on either end of each conductor for a total of four ports which were then configured into two differential ports, one for each side. Simulation results thus provide a set of differential 2-port S-parameters for the given length of transmission line. Over a wide frequency range, the *RLGC* parameters are frequency dependent, however, over a narrow frequency range we can assume they are relatively constant. The optimization seeks to find an optimum resonator only at 60 GHz so that the calculations can be limited to a narrow bandwidth and we can safely assume constant *RLGC* parameters. Thus, we only need to simulate the S-parameters at one frequency point and extract the line's *RLCG* parameters from that point alone. This conversion is performed in multiple steps. First,

the S-parameters must be converted into $ABCD$ parameters using Eq. 2.13-2.16.

$$A = \frac{(1 + S_{11})(1 - S_{22}) + S_{12}S_{21}}{2S_{21}} \quad (2.13)$$

$$B = Z_0 \frac{(1 + S_{11})(1 + S_{22}) - S_{12}S_{21}}{2S_{21}} \quad (2.14)$$

$$C = \frac{1}{Z_0} \frac{(1 - S_{11})(1 - S_{22}) - S_{12}S_{21}}{2S_{21}} \quad (2.15)$$

$$D = \frac{(1 - S_{11})(1 + S_{22}) + S_{12}S_{21}}{2S_{21}} \quad (2.16)$$

Next, Z_0 and Γ are computed from the $ABCD$ parameters using Eq. 2.17 and Eq. 2.18.

$$Z_0 = \sqrt{\frac{B}{C}} \quad (2.17)$$

$$\Gamma = \frac{\operatorname{arccosh}(A)}{l} \quad (2.18)$$

The resulting $|Z_{0,diff}|$ profile over the design space is shown in Fig. 2.5. The contours show that the characteristic impedance of a differential CPS transmission line is strongly dependent on width when the spacing is large but only weakly dependent on width when the spacing is small. Finally, the $RLGC$ parameters can be extracted from Z_0 and Γ using Eq. 2.19-2.22.

$$R = \Re(Z_0\Gamma) \quad (2.19)$$

$$L = \frac{\Im(Z_0\Gamma)}{\omega} \quad (2.20)$$

$$G = \Re\left(\frac{\Gamma}{Z_0}\right) \quad (2.21)$$

$$C = \frac{\Im\left(\frac{\Gamma}{Z_0}\right)}{\omega} \quad (2.22)$$

This process can be repeated for every combination of spacing and width within the design space although this is not strictly necessary as results can be interpolated very accurately between simulated points if the gradient in the region is small. The bounds of the design

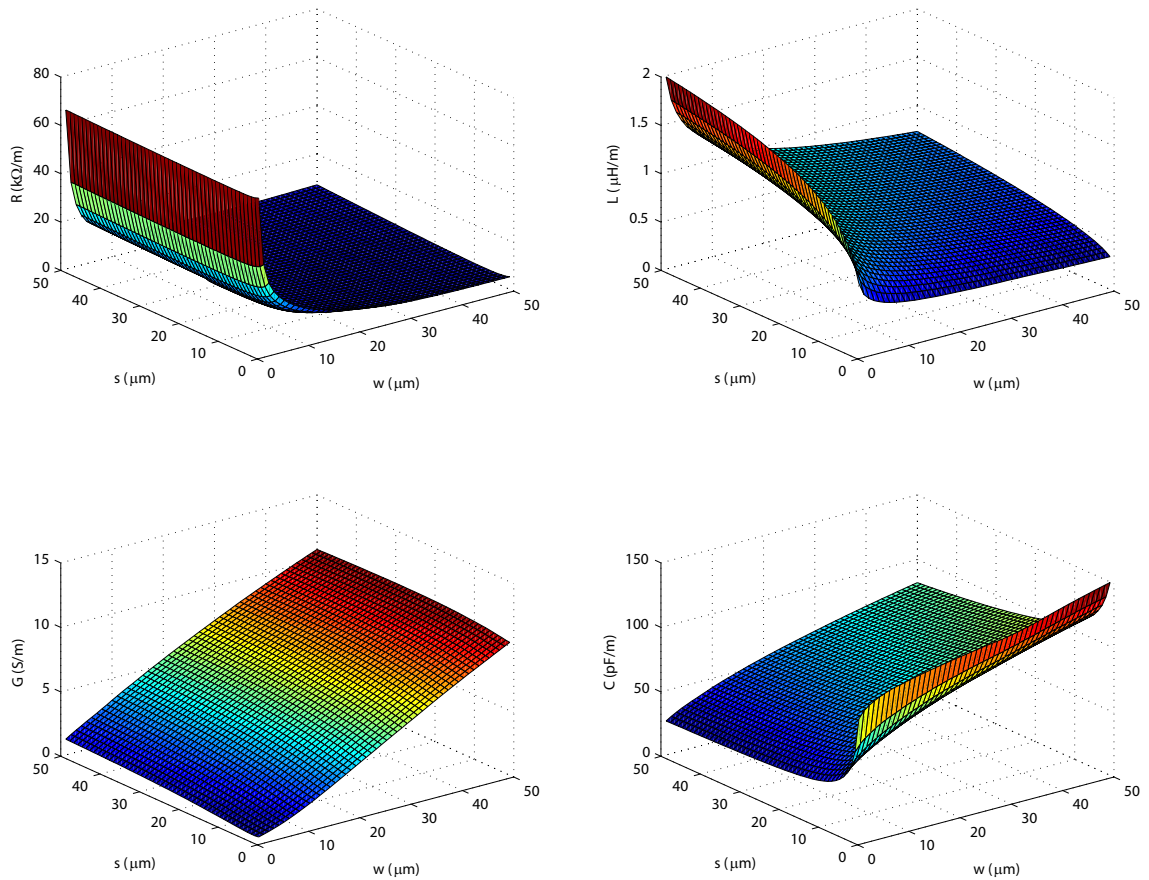


Figure 2.6: $RLCG$ per meter for a uniform differential stripline.

space are determined by the maximum width and spacing required in the final tapered resonator. Since this was not known a priori, a choice of $50\mu\text{m}$ was made for the maximum width and spacing. As will be shown by the optimization results in section 2.3.3, this choice proved to be satisfactory. The $RLCG$ parameters for the differential stripline over the design space are shown in Fig. 2.6.

Even before the actual optimization we can see from Fig. 2.6 that some of our earlier intuition makes physical sense. The series resistance is strongly dependent on the

conductor width and only weakly dependent on the spacing. As the conductor becomes wider, the series resistance initially drops very rapidly but then settles to an almost constant value. This is because skin effect at these frequencies limits the minimum resistance that can be achieved and the differential operation of the transmission line creates current crowding along the inner edges meaning little or no current flows on the outer edges. Thus, as the conductor is made wider extra metal is added where no current is flowing so the effective resistance is not actually changed. Conductor spacing only affects the series resistance when the conductors are very close together due to proximity effects which increase current crowding on the inner edges. This raises the effective series resistance. As the conductors are pulled apart this effect diminishes very rapidly, becoming insignificant.

The shunt conductance is also strongly dependent on the conductor width. Wider metals lead to more capacitive coupling to the conductive substrate which in turn increases the shunt conductance between the differential lines. Inductance is mainly determined by the spacing of the lines, or put another way, the enclosed loop area. Shunt capacitance is dominated by the parallel plate capacitance between the metal lines when they are close together and fringing capacitance when they are far apart. As the metal is made wider, fringing capacitance increases, raising the overall shunt capacitance.

As a final note, the transmission line length, l , is kept the same for each simulation for simplicity but this does not affect the results since Γ is normalized before computing the *RLGC* parameters. The choice of the actual length, however, is governed by the frequency of interest. A short line may not provide accurate results if the correct transmission line mode cannot be established in the simulation. A long line, on the other hand, may give

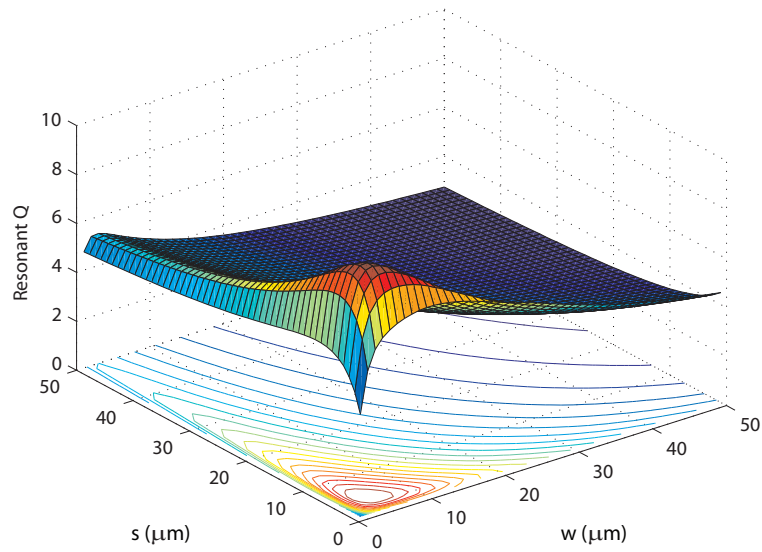


Figure 2.7: Resonant Q of quarter wavelength uniform differential stripline.

incorrect results if its length is close to an integer multiple of half the wavelength at the frequency of interest. This is because the simulation setup is that of an open ended stub which exhibits a parallel resonance mode when its length is equal to an integer multiple of half the wavelength. The mathematical equations used to extract *RLGC* models in Eq. 2.13-2.22 become inaccurate near the frequency at which this occurs since the numbers involved can become very large or very small. Thus, it is prudent to maintain a length less than half a wavelength to avoid resonance effects, but at least one fifth the wavelength to ensure a transmission line mode is established in the simulation.

2.3.2 Optimization Methodology

The first step in the optimization is to find the optimum uniform resonator as a reference. The resonant Q of a shorted quarter wavelength uniform transmission line

resonator can be found using Eq. 2.23 and the values of Γ computed earlier during the *RLGC* model extraction.

$$Q = \frac{\beta}{2\alpha} = \frac{\Im(\Gamma)}{2\Re(\Gamma)} \quad (2.23)$$

The result of this computation for all the points in the design space is shown in Fig. 2.7. Thus, finding the optimum uniform resonator is as easy as finding the maximum of Fig. 2.7. In this case the optimum width and spacing are both $5 \mu m$ and the resulting Q is approximately 9.5. This is in line with measured data of transmission lines in this process and will be the reference Q for the optimization to follow.

The uniform resonator is first split up by choosing a number of equally spaced vertices along its horizontal length which are used to set the width and spacing at those positions. At every other point the width and spacing are interpolated from the known values at the vertices. The optimization variables are thus the width and spacing values at each vertex and the overall resonator length which is used as a scaling factor for the horizontal vertex positions. This is necessary because β will not be constant over the length of the tapered resonator and thus the quarter wavelength at 60 GHz will vary as the tapering is varied. The initial values for all vertices are set to the optimal width and spacing for a uniform resonator and the length is set to the nominal quarter wavelength at 60 GHz.

To find the optimum tapered resonator, all optimization variables are jointly optimized. This requires an iterative approach whereby the voltage and current profiles along a given taper shape are first found by numerically solving Eqs. 2.3 and 2.4, followed by an optimization of the shape to those particular voltage and current standing waves with the goal of maximizing Eq. 2.12. The distortion of the taper shape changes the voltage and

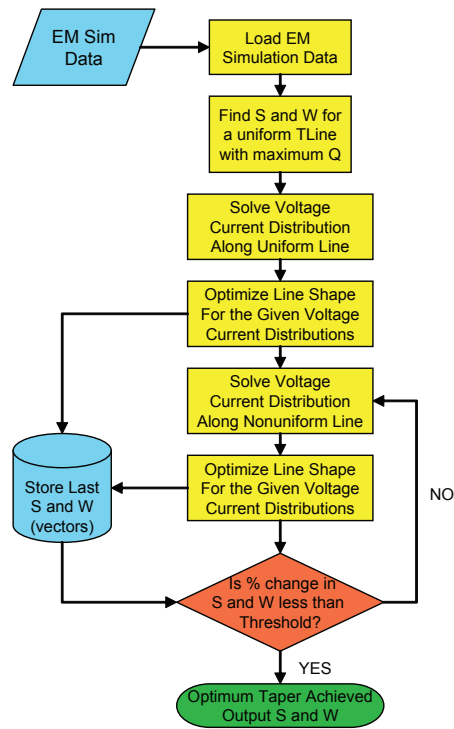


Figure 2.8: Tapered resonator optimization flow chart.

current profiles so they must be recomputed once the optimum shape has been found. The taper shape is then optimized to the new voltage and current standing waves. This process continues iteratively until the taper shape converges to an optimum. Random starting points are utilized and multiple runs are averaged to increase the probability of reaching a globally optimal shape. A flow chart of the entire process can be seen in Fig. 2.8. It must be noted, however, that all of the above calculations assume that a perfect short ($R = 0, L = 0$) is present at the end of the resonator. In the actual implementation a real short would have nonzero resistance and inductance and will change the results somewhat. It is expected that the center frequency of the resonator will be shifted down in frequency due to the additional unaccounted series inductance.

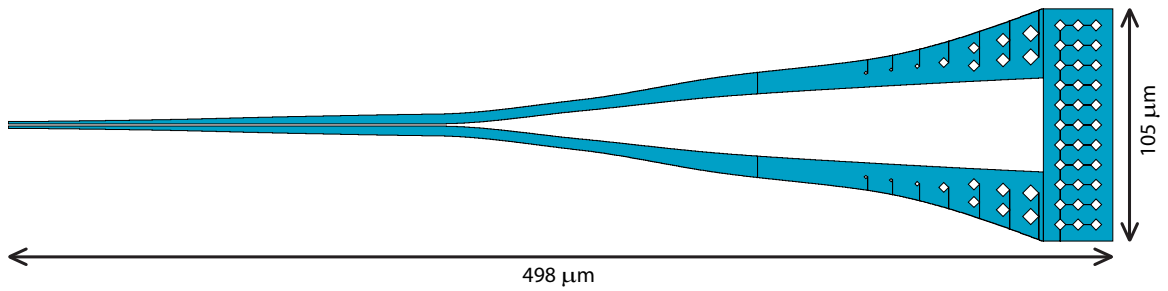


Figure 2.9: The layout of the optimized quarter wave line. The characteristic impedance Z_0 is non-constant. Slotting is introduced to satisfy design rules.

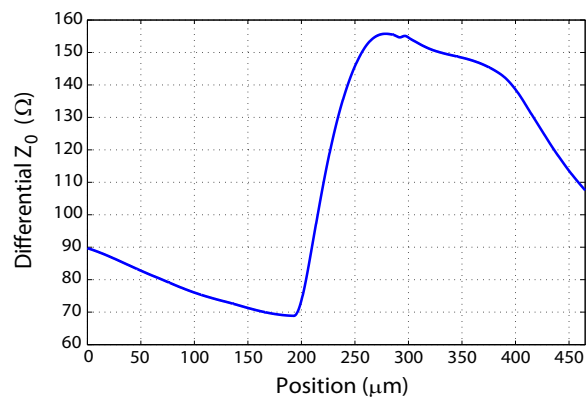


Figure 2.10: The optimum characteristic impedance Z_0 profile.

2.3.3 Optimization Results

The optimum shape derived by the method described in section 2.3.2 is shown in Fig. 2.9 and has the characteristic impedance profile shown in Fig. 2.10. According to the Matlab calculations this shape should have a quality factor of just over 15, an improvement of more than 60% compared to the uniform resonator. As mentioned in section 2.3.2, the optimization averaged multiple runs with random starting points to arrive at this optimal shape. Most of the results were nearly identical in shape and quality factor, while the outliers achieved significantly lower quality factors and were thus eliminated before averaging.

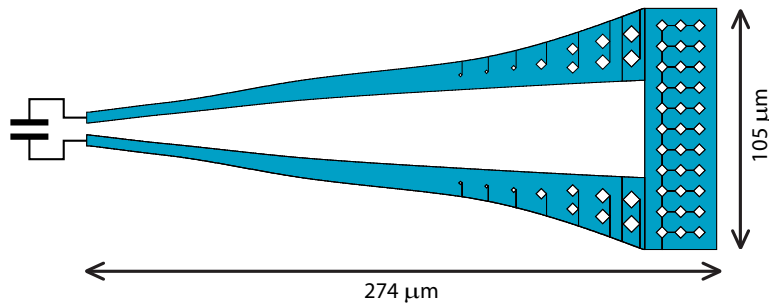


Figure 2.11: The layout of the optimized capacitor loaded half-resonator. The characteristic impedance Z_0 is non-constant. Slotting is introduced to satisfy design rules.

Interestingly, the resulting characteristic impedance is not constant, but varies widely over the length of the resonator. The sharp step in characteristic impedance shows that the transmission line is more capacitive for the left half where most of the energy is stored in the electric field than the right half where most of the energy is stored in the magnetic field. This is clearly reminiscent of an LC tank with the left half of the resonator representing a distributed capacitor and the right half, a loop inductor. This step is also the point where the dominant losses change from resistive to conductive. Unfortunately, this result presents a problem for implementation into a VCO where the resonant tank is usually used to bias the VCO core and thus must carry a DC current. The very narrow metal widths present in the left half of this resonator would cause a large DC voltage drop. However, we can take advantage of the realisation that the left half of the resonator is essentially just a distributed capacitor which can be replaced by a lumped capacitor. The equivalent capacitance can be found by integrating $C(x)$ over the left-half of the resonator as shown in Eq. 2.24.

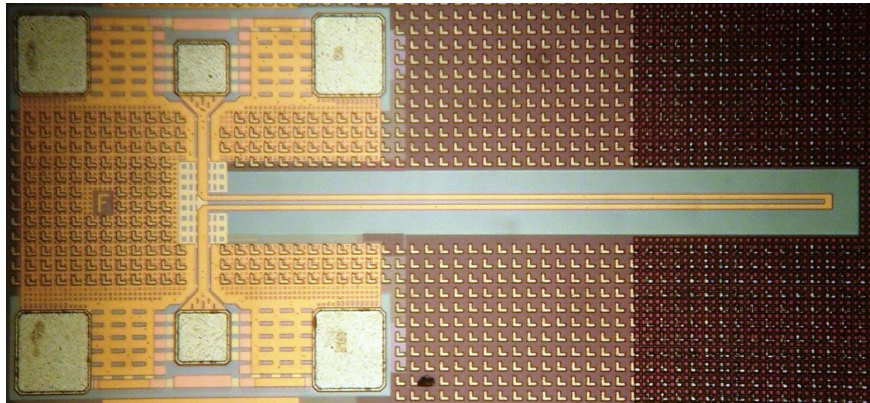
$$C_{eff} = \int_{-L}^{-\frac{L}{2}} C(x') dx' \quad (2.24)$$

Replacing the left half of the resonator with a lumped capacitor also reduces the area occupied by the resonator and, depending on the quality of the capacitor, can reduce overall losses leading to higher resonator Q . Conceptually, this is shown in Fig. 2.11. Due to the availability of MIM capacitors in our process we chose this type for the actual implementation due to their high quality factor and capacitance density.

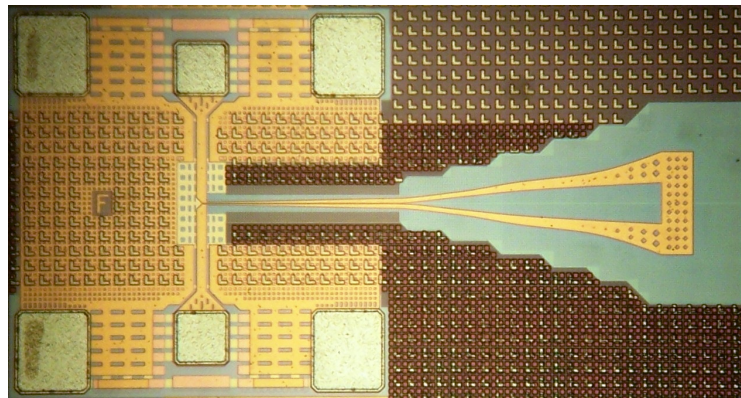
To verify the Matlab computations, HFSS was used to simulate all three versions of transmission line resonator: uniform, tapered, and half-taper. The shorted half resonator by itself simply acts like an inductor so its simulation results are placed in parallel with a capacitor with a Q of 40 at 60 GHz and a capacitance computed using Eq. 2.24. These results will be shown alongside measurements for comparison in section 2.4.

2.4 Experimental Results

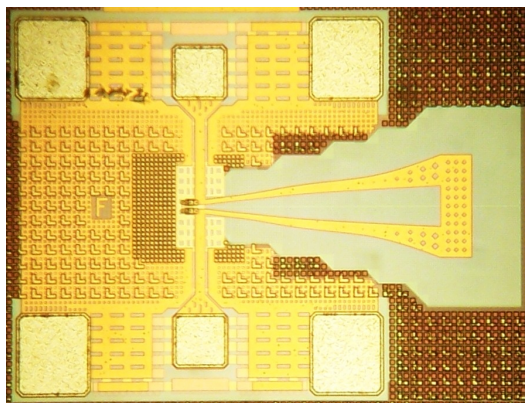
All three resonator versions were fabricated in a standard 90nm digital CMOS process with no RF options. The transmission line resonators shown in Figures 2.9 and 2.11 are shown without the interface that would be required to connect them to the VCO core. In most cases this interface would involve vias down to lower metal layers and routing leading to the actual transistors in the VCO core. This interface must always be taken into account in the design but in the case of characterizing the resonator alone we must interface it to an appropriate pad structure. In this case, due to the lack of high frequency differential pads, the measurement had to be done with two single ended ground-signal-ground (GSG) pads. Due to physical limitations on the probe station the pads had to be positioned directly opposing each other. Unfortunately, each pad layout has a built in section of 50Ω



(a) Uniform resonator



(b) Tapered resonator



(c) Capacitor-loaded tapered half-resonator

Figure 2.12: Layout of resonator test structures.

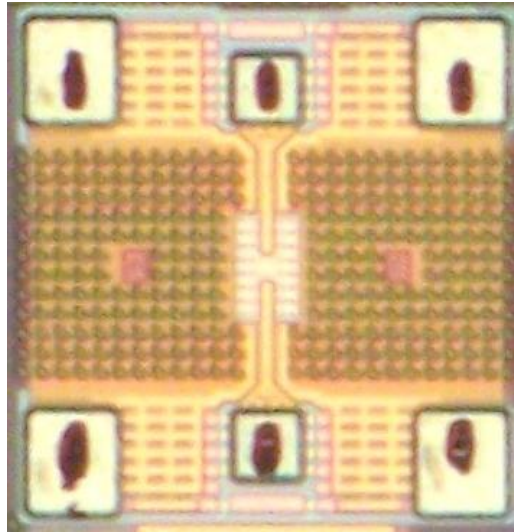


Figure 2.13: Layout of deembedding structure.

CPW transmission line which is $40\mu\text{m}$ long which must in turn interface to one side of the differential CPS resonator. Thus, care must be taken to reduce reflections along this interface by keeping the characteristic impedance as close as possible to 50Ω . At the same time it is imperative that any interface does not change the behavior of the resonator itself or affect its performance. To this end, a microstrip transmission line provides the easiest and most unobtrusive interface to CPS. The CPW transmission lines built into the pads first transition to microstrip transmission lines which extend out to the resonator meeting it at a 90 degree angle. The microstrip is formed by placing the signal line in the top metal layer and a ground plane in the bottom metal layer. The microstrip signal lines are then directly connected to the differential CPS and the grounds are connected to each other but removed from directly underneath the CPS so as to not affect resonator performance.

The final test structure layouts for the uniform, tapered, and capacitor-loaded

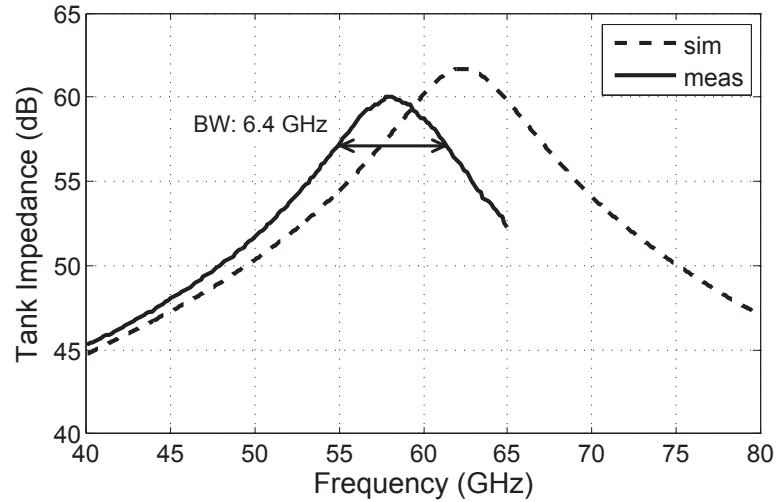


Figure 2.14: Measured and simulated impedance for the uniform resonator.

tapered half-resonators are shown in Figures 2.12(a), 2.12(b), and 2.12(c) respectively. An open-short deembedding procedure is used to remove the effects of the pads, CPW and microstrip transmission lines, and all associated transitions. The layout of a deembedding structure used for this procedure is shown in Fig. 2.13. This layout has to include the pads and microstrip transmission lines in an identical configuration to that used in the resonator test structures. For the open deembedding structure the microstrip signal lines are left floating, while for the short deembedding structure vias are placed to connect the signal lines to the ground plane below.

Figures 2.14, 2.15, and 2.16 show the measured and simulated absolute value of impedance versus frequency for the uniform, tapered, and capacitor-loaded resonators respectively. A systematic offset of approximately 4 GHz is present for all resonator versions, due to deembedding inaccuracies and some process variations which will be explained in section 2.4.1. However, the quality factor is consistent with simulation. Table 2.1 summa-

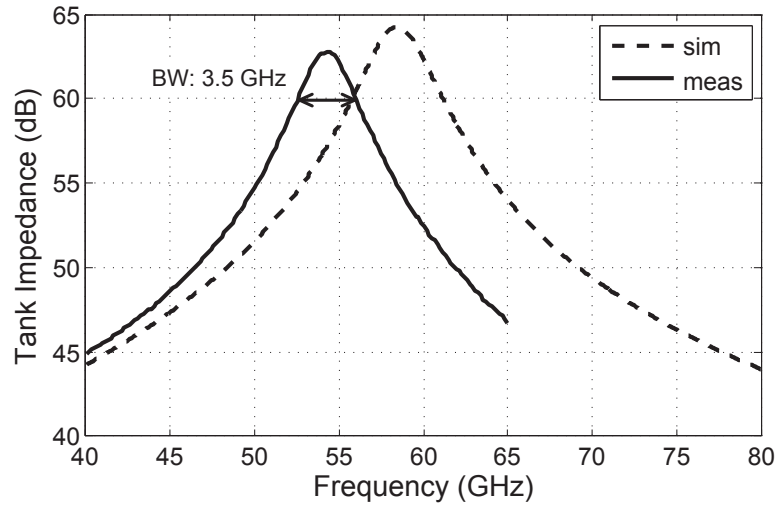


Figure 2.15: Measured and simulated impedance for the tapered resonator.

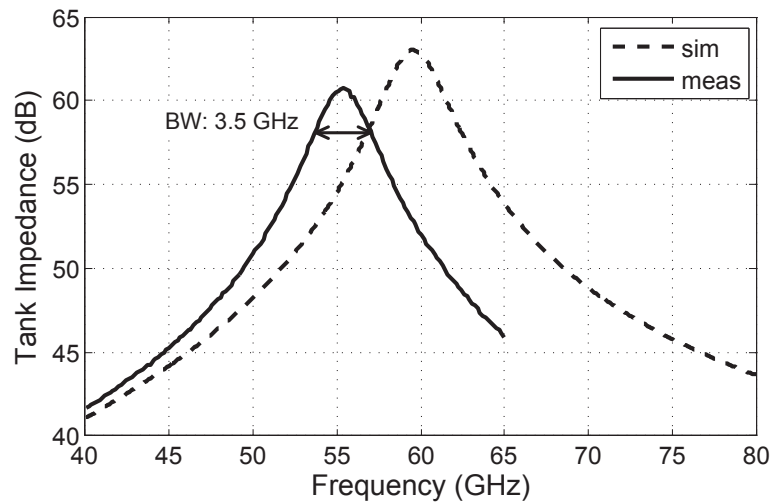


Figure 2.16: Measured and simulated impedance for the capacitor-loaded tapered half-resonator. (Capacitor Q is assumed to be 40 in simulation.)

<i>Resonator Type</i>	f_0 (GHz)	Q	ΔQ
Uniform (ref.)	57.9	8.8	–
Tapered	54.4	15	70.4%
Cap-Loaded Half-Taper	55.4	15.1	71.6%

Table 2.1: Measurement Results

rizes the measurement results for the three types of resonators. Interestingly, while both versions of tapered resonators exhibited quality factors extremely close to those predicted by Matlab simulations, the quality factor of the uniform resonator came out slightly lower than expected.

Measurement results show a 70% improvement in Q over the uniform resonator using our optimization, slightly better than predicted by Matlab computations. We believe that the increased substrate losses present at 60 GHz prevent us from achieving further improvements. However, using a lower loss substrate or operating at a lower frequency could allow Q improvements of well over 100%. While a thicker metal option would not necessarily help at our current frequency, due to skin effect, at lower frequencies the skin effect would decrease and thicker metal options would certainly be advantageous.

2.4.1 Accounting for Deembedding Inaccuracies

As mentioned above in section 2.4, an open-short deembedding procedure was used to remove the effects of pads, transmission lines and transitions leading up to the resonator. This procedure requires the measurement of “open” and “short” deembedding structures. These structures must be identical to the ones used in the resonator test structure except the resonator itself is replaced with an open circuit and short circuit respectively. Unfortunately, a layout error is present in the deembedding structures of the test chip used for this research which caused a small portion of microstrip line to not be deembedded. As mentioned above in section 2.4, the deembedding structures must be identical to the test structures in all aspects while omitting only the actual device to be deembedded. In this case, however, the microstrip transmission line in the deembedding structure was made shorter than in the

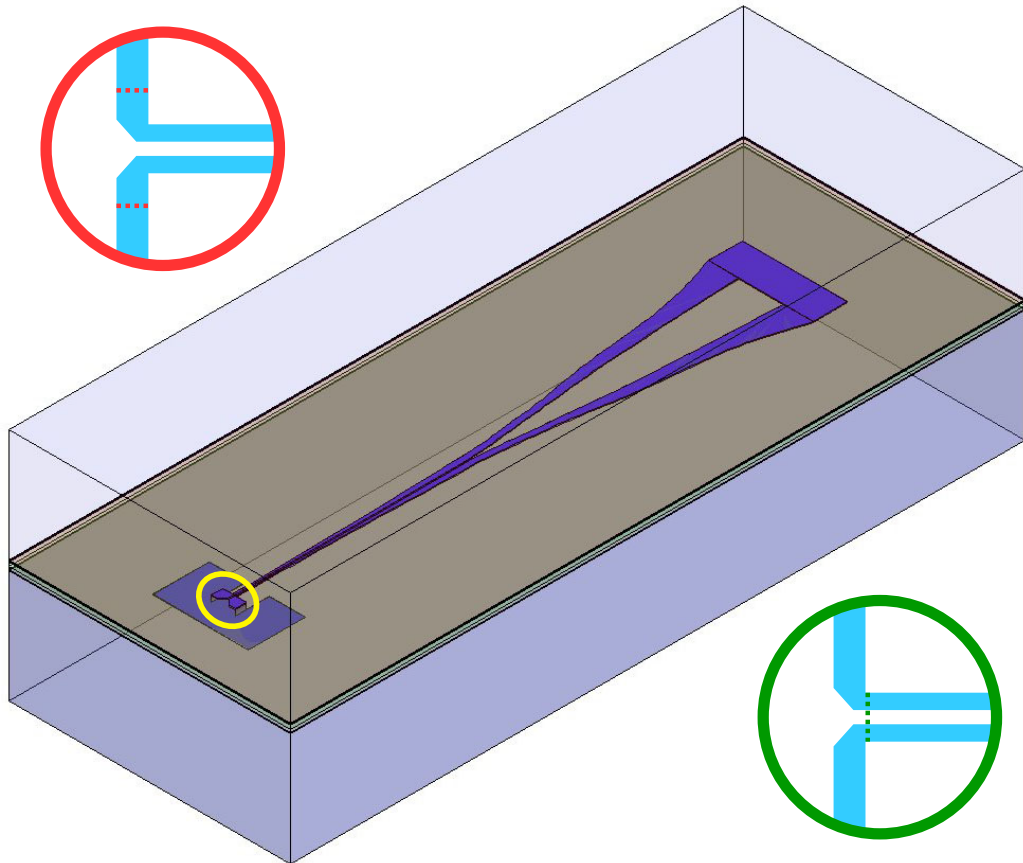


Figure 2.17: Tapered resonator 3D layout model in HFSS including undeembedded interconnect and microstrip to CPS transition. The two insets show the actual extent of deembedding (left) compared to the expected deembedding (right).

test structures and did not include the 45° taper of the microstrip to CPS transition which can be seen in the test structure layouts in Fig. 2.12. In order to have a fair comparison between measurement and simulation, this layout error must be taken into account in simulation. Fig. 2.17 shows the HFSS 3D model of the tapered resonator including the section of microstrip transmission line which was not deembedded. The inset on the right hand side shows the expected deembedding down to the actual resonator, seen extending out to the right. The left inset, on the other hand, shows the actual extent of deembedding which left a portion of microstrip transmission line. Fig. 2.18 shows the absolute value of impedance versus frequency comparing the measured value to the new HFSS simulation. Clearly, the layout error accounts for most of the frequency offset seen in Figures 2.14, 2.15, and 2.16.

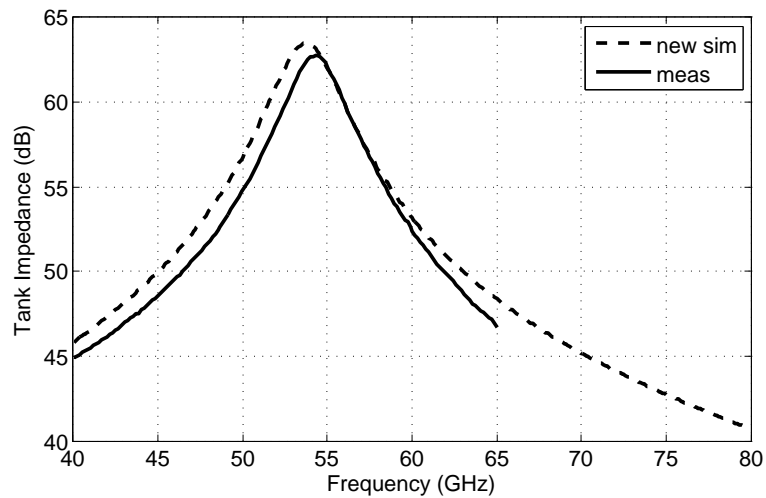


Figure 2.18: Measured and simulated impedance for the tapered resonator taking into account the deembedding structure layout error.

2.5 Comparison to lumped LC tank

At low frequencies, distributed components such as the tapered resonator presented here are simply too large to integrate on-chip since their size is on the order of the wavelength at the frequency of interest, thus, leading to the use of lumped components. However, as frequencies of operation scale higher, distributed components become a viable option since the wavelength decreases. In this section we will determine whether or not it is beneficial to use distributed over lumped components at 60 GHz in our 90nm digital CMOS process. The tapered resonator can be directly compared to a lumped LC tank. As we saw in section 2.4, replacing the distributed capacitance represented by the left half of the tapered resonator with a high quality MIM capacitor had no effect on the overall resonator Q. The remaining section of tapered resonator acts like an inductor so we can directly compare its inductive quality factor to that of a lumped inductor in the same process. Standard, single turn, octagonal inductors with various diameters and conductor widths were simulated in HFSS using a single differential port across the two terminals in the same method used for the tapered resonators, and using the same substrate. A sample simulation setup is shown in Fig. 2.19. For simplicity, we model the inductor as a resistor in series with an inductor as shown in Fig. 2.20. In this way, the inductance and the quality factor can be easily extracted from simulation using Z-parameters. The 1-port S-parameters from the HFSS simulations are first converted to Z-parameters using Eq. 2.25.

$$Z_{11} = Z_0 \frac{1 + S_{11}}{1 - S_{11}} \quad (2.25)$$

Since this is a 1-port system, Z_{11} represents the impedance seen across that port. Thus, we can use Eqs. 2.26 and 2.27 to find the equivalent inductance and its inductive quality

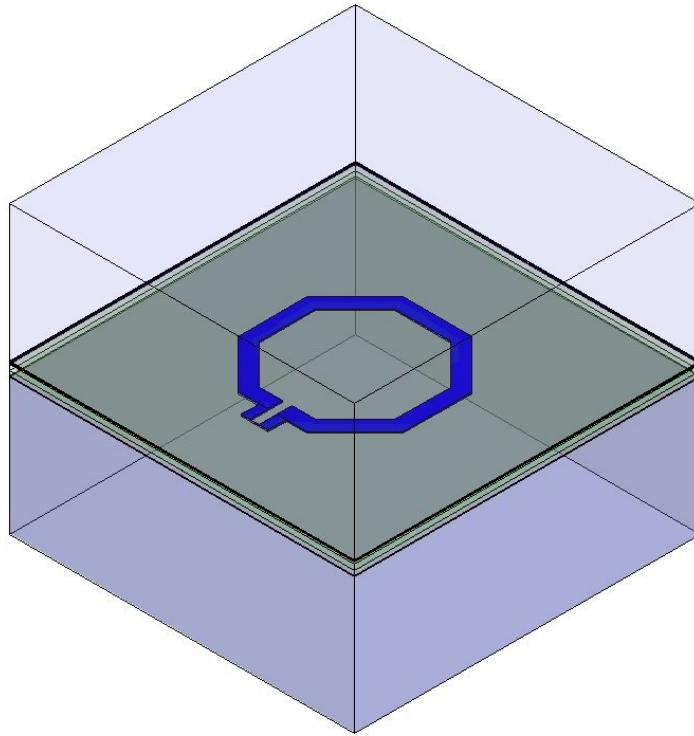


Figure 2.19: Single turn octagonal inductor layout in HFSS using only the top metal layer.

factor, respectively. This same method can be used to find the equivalent inductance and inductive quality factor of the half-taper resonator.

$$Q_{ind} = \frac{\Im(Z_{11})}{\Re(Z_{11})} \quad (2.26)$$

$$L = \frac{\Im(Z_{11})}{\omega} \quad (2.27)$$

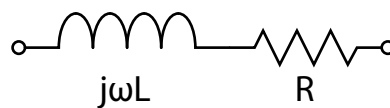


Figure 2.20: Simple inductor model taking into account series losses.

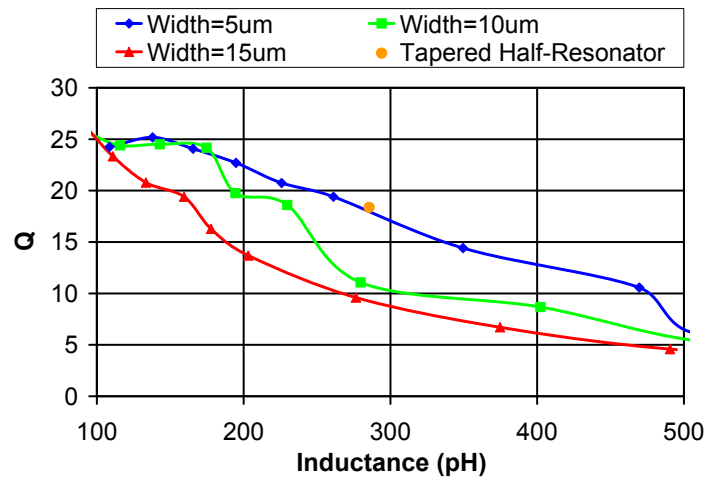


Figure 2.21: Inductive Q versus inductance comparison between standard single turn octagonal inductors and tapered half-resonator.

To create a fair comparison, the quality factor was plotted versus the equivalent inductance for each lumped inductor and for the half-taper resonator in Fig. 2.21. Unfortunately, it seems that the tapered half-resonator is no better than an optimized, standard, single turn octagonal lumped inductor. It is important to note that the diameters required in the lumped inductor lead to a comparable but smaller overall area than the tapered transmission line. These findings show that optimized inductors with MIM capacitors can perform as well as optimized transmission line resonators at 60 GHz in our particular process while occupying much less area.

Chapter 3

Conclusion

An optimum tapered transmission line resonator for 60 GHz applications was presented using a differential stripline on a standard digital 90nm CMOS process with no RF options. A comprehensive optimization approach was utilized to achieve the optimum taper shape without any constraint on the characteristic impedance. The only constraints on the design were due to design rules in our process which limited the minimum line widths and spacings. This approach presents a transmission line resonator with a Q of 15, an improvement of 70% over an optimum uniform resonator. This approach also has the potential for much higher Q gains if lower loss substrates are available or at lower frequencies. A capacitor-loaded tapered half-resonator was also developed and shown to have the same Q improvement as its larger cousin while occupying much less area and reducing common mode DC losses. This version would be very useful in the design of an integrated VCO since it could be used to bias the VCO core without significant common mode DC voltage drop. Another possible solution would be an open ended half wavelength resonator. This

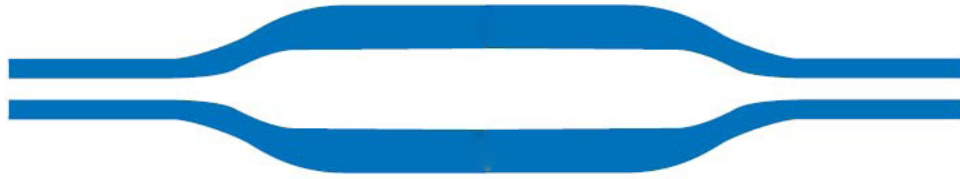


Figure 3.1: A tapered open ended half wave transmission line utilizes wide width and large gap spacing when the current is high (voltage is low) and narrow width and small gap when the voltage is high (current is low).

arrangement is a trivial extension of this work since it can be seen as two quarter wavelength resonators connected back to back as shown in Fig. 3.1. An additional advantage of this is that an actual short between the two lines would not need to be provided since the horizontal midpoint is a differential ground. The midpoint could be connected to the supply voltage to bias up the VCO core but this interconnect could have a high inductance since it would not have to also support signal currents. However, it was also shown that the tapered resonators presented are currently no better than lumped components in quality factor yet consume more area. At higher frequencies perhaps the balance will shift in favor of distributed components. Nevertheless, it is possible that slow wave techniques could help improve the quality factor of transmission line based resonators even at 60 GHz. This approach was not explored during this research but work done in [4] shows that further improvements could be possible with slow wave structures. Moreover, the use of such slow wave structures would reduce the overall area occupied by the resonator and could make it comparable to, or smaller than, the area of a lumped LC tank.

Other possible applications of this work include filters and transmission line matching networks which utilize open and short shunt stubs. In filter applications transmission line stubs would be used to replace LC tanks and would therefore be quarter or half wave-

length depending on the particular filter. Stubs used in matching networks, on the other hand, are not necessarily a quarter or half wavelength since they must synthesize a different impedance for each particular application. Nevertheless, the loss of these stubs adversely affects the loss of the overall matching network. Therefore, the approach presented here could be used to reduce the losses of matching transmission line stubs with some modifications. Unlike resonators which look like parallel LC tanks, stubs must present a certain imaginary impedance thus looking like either a capacitance, or an inductance. The optimization goal would therefore need to be changed to take this into account. Instead of optimizing for maximum resonant Q given a required center frequency, the goal would be to maximize either capacitive or inductive Q , given a certain value of capacitance or inductance, respectively. This approach has not been investigated in detail and would be a good topic for further research.

Bibliography

- [1] D.B. Leeson, "A Simple Model of Feedback Oscillator Noise Spectrum," *Proceedings of the IEEE*, vol. 54, pp. 329-330, 1966.
- [2] R. E. Collin, "The Optimum Tapered Transmission Line Matching Section," *Proceedings of the IRE*, vol. 33, issue 4, pp. 539-548, Apr. 1956.
- [3] W. F. Andress and D. Ham, "Standing Wave Oscillators Utilizing Wave-Adaptive Tapered Transmission Lines," *IEEE J. Solid-State Circuits*, vol. 40, no. 3, pp. 638-651, Mar. 2005.
- [4] H. Krishnaswamy, H. Hashemi, "A 26 GHz coplanar stripline-based current sharing CMOS oscillator," *IEEE Radio Frequency Integrated Circuits Symposium 2005, Digest of Papers*, pp. 127-130, Jun. 2005.
- [5] D. M. Pozar, *Microwave Engineering*, John Wiley & Sons, 2004.
- [6] R. E. Collin, *Foundations for Microwave Engineering*, Wiley-IEEE Press, 2000.
- [7] D. C. Youla, "Analysis and Synthesis of Arbitrarily Terminated Lossless Nonuniform

- Lines,” *IEEE Transactions on Circuits and Systems*, vol. 11, issue 3, pp. 363-371, Sep. 1964.
- [8] C. P. Womack, “The Use of Exponential Transmission Lines in Microwave Components,” *IRE Transactions on Microwave Theory and Techniques*, vol. 10, issue, 2, pp. 124-132, Mar. 1962.
- [9] K. Lu, “An Efficient Method for Analysis of Arbitrary Nonuniform Transmission Lines,” *IEEE Transactions on Microwave Theory and Techniques*, vol. 45, issue, 1, pp. 9-14, Jan. 1997.